BeBeC-2024-D08

RELIABLE CAR PASS-BY SOURCE LEVELS FROM MICROPHONE ARRAY DATA

Mikołaj Czuchaj[1] and Ennes Sarradj[2]
[1]Fachgebiet Technische Akustik, TU Berlin, Einsteinufer 25, 10587 Berlin, Germany

Abstract

The paper discusses the use of the CLEANT time-domain deconvolution algorithm for car pass-by measurements. One advantage of using this more elaborated algorithm is its higher and nearly frequency-independent spatial resolution. Moreover, this algorithm allows spatial integration over the map for a detailed estimation of absolute levels for the contribution of all individual sources. The application of the CLEANT algorithm in this context requires adaptations for constructing an overall map from partial results. These adaptations are implemented based on the Acoular Python library. To demonstrate the algorithm, a dataset with approximately 50 pass-by measurements is used. This dataset comprises two different cars and a pass-by speed range between 30 km/h and 80 km/h. The results not only allow to assess the contribution from individual sources but also their speed dependence. This offers valuable insight into source mechanisms, which is essential for developing effective noise mitigation strategies and enhancing vehicle design for reduced acoustic impact.

In conclusion, this paper highlights the potential of microphone array technology together with state of the art signal processing methods as a versatile tool for pass-by noise measurement, offering improved spatial resolution, accuracy, and insight into the acoustic behavior of vehicles. The findings contribute to advancing the state-of-the-art in vehicle noise assessment and may provide a foundation for future research and standardization efforts in this field.

1 Introduction

Pass-by noise assessment plays a crucial role in evaluating the acoustic impact of vehicles on the environment and human health. Established methods often rely on single-point measurements, which do not provide information on which sources contribute how much to the overall noise level. Using a microphone array can be instrumental in locating the sources and estimating their contributions. Consequently, a number of microphone array applications for pass-by noise have been reported in the last 20 years. One common pitfall that is often observed is the lack of comparability of the microphone array results to those from standard single-point measurements. The reason for this is that the beamforming algorithms used for moving sources produce results with a frequency-dependent spatial resolution, which also influences the absolute source levels that can be derived from the results.

Examples of using microphone arrays to study traffic noise are abundant across various domains, including the investigation of aircraft noise [9, 13] and train noise [8, 10]. Recently, the authors developed a method based on the CLEANT technique [4] to investigate high-speed train pass-by noise [5–7]. This method has been demonstrated within the scope of the EU project S2R TRANSIT (881771) [14–16], where it was applied in multiple high-speed train noise assessments.

The advantage of this method lies in its ability to remove the influence of the point spread function through deconvolution. This allows for a quantitative analysis of source areas through spatial integration in the source maps, as well as precise source localisation. The method also takes into account other effects that occur due to source motion, such as the Doppler effect and convective amplification.

In the current study, the application of this method is extended to the analysis of car pass-by noise, thereby broadening its scope and demonstrating its versatility. The measurement data utilized in this analysis is sourced from research conducted by Ballesteros et al. [1, 2], wherein it was previously analyzed using beamforming techniques with a moving focus.

2 Measurements

The measurement setup is depicted in Figure 1, showing an annotated photograph of the measurement as well as the microphone array geometry. The microphone array consisted of a planar array with 56 microphones, to which an additional 28 microphones were attached using 8 arms, resulting in a total of 84 microphones. The microphone array geometry was optimised as described in [1].

The array was positioned at a distance of 5 metres from the measurement area, which was defined by two light barriers in a distance of 10 metres to each other. Measurements began when the vehicle activated the first light barrier and ended after it activated the second light barrier and traveled an additional five metres. Data was collected at a sampling frequency of 25,600 Hz. Additionally, temperature and wind speed were monitored using a weather station. The temperature varied between 23 and 25 degrees Celsius, and the wind speed was less than 3 km/h.

Two different vehicles were tested: a petrol-powered 2009 Skoda Octavia with 195/65 R15 91H tyres and a diesel-powered 2005 Toyota Avensis with 205/55 R16 91V tyres. An overview of the measurements taken, along with the driving speeds and gears used, is provided in Table 1.

Car	**Pass-bys**	**min. Velocity (km/h)**	**max. Velocity (km/h)**	**Used Gears**
Skoda Octavia	33	30	80	2, 3, 4, 5, 6
Toyota Avensis	13	30	80	3, 4, 5, 6

Table 1: Summary of car pass-bys with corresponding velocities and gears used.

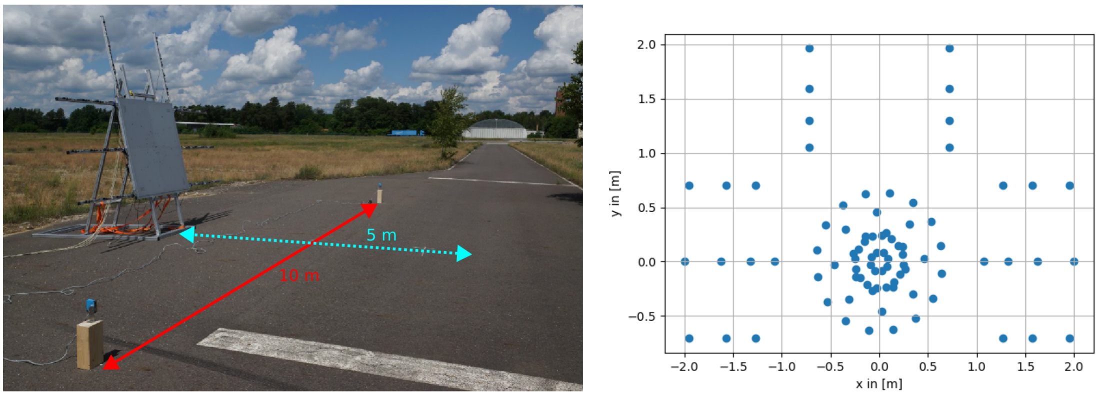

Figure 1: A photograph of the measurement setup (left). The distance between the array and the measurement area is marked with a dotted light blue line, and the distance between the light barriers is indicated by a red line. The array geometry, consisting of 84 microphones, is shown (right).

The passes were carried out at a constant speed of 30 km/h to 80 km/h, with the vehicle passing the microphone array both from left to right and vice versa. This procedure was chosen to comply with the ISO 362 standard [3]. To enable a consistent comparison between the two vehicles, the following gear selections were used: third gear at 30 km/h, fourth gear at 40 km/h, fifth gear at 50 km/h, and sixth gear at 60 km/h and above.

3 Method

3.1 Beamforming with Moving Focus

The Delay-and-Sum Beamforming on a moving grid forms the basis for the CLEANT method. The method consists of summing a series of delayed sound pressure signals p_m on a moving grid of focus points x_g. The method determines the sound pressures at the center of the array or at a specified distance from the grid point, contributed by sources at these points at a time t. The beamforming output at a time t and focus point x_g is given by the Equation (1), where p_m is the sound pressure, w_m is the spatial weighting coefficient of the m-th microphone, $\theta_{x_g,m}$ is the motion angle, r_{x_gm} is the time-dependent source-sensor distance, M is the Mach number, K_{x_g} a normalization term, and c the speed of sound.

$$b(t, x_g, p_m) = \frac{1}{K_{x_g}(t)} \sum_{m=1}^{N} w_m \frac{p_m(t + \frac{r_{x_gm}(t)}{c})}{r_{x_gm}(t)(1 - M\cos(\theta_{x_gm}(t)))^2} \tag{1}$$

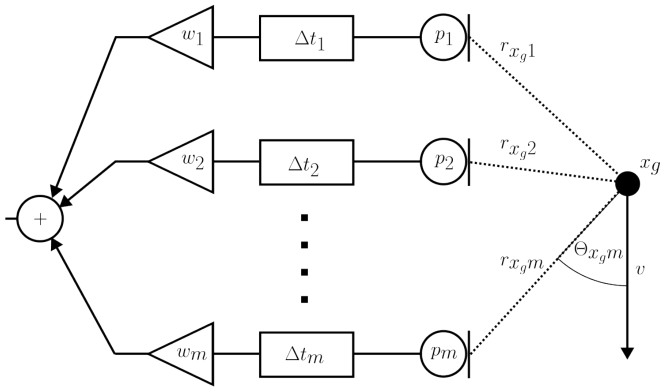

Figure 2: Principle Sketch of beamforming on a moving grid.

The normalisation term is defined as:

$$K_{x_g}(t) = \sum_{m=1}^{N} \frac{w_m}{[r_{x_gm}(t)(1 - M\cos(\theta_{x_gm}(t)))^2]^2}. \tag{2}$$

The principle is shown in Figure 2, where the microphone signals p_1 to p_m are summed at the grid point x_g.

3.2 CLEANT Method

The CLEANT method proposed by Cousson et al. [4] aims to remove the influence of the point spread function. This leads to better spatial resolution in acoustic maps and enables the calculation of the source strength by spatial integration on the map. It is based on delay-and-sum beamforming and iteratively finds a clean representation of the original beamforming result. The method is performed on a moving grid, which allows the Doppler effect to be removed and convective amplification to be taken into account. The main goal of the method is to find a clean representation of the result from the delay-and-sum beamforming map. In a first step, an initialization of a beamforming map $\Phi^{(0)}$, a clean representation $\Gamma^{(0)}$ and the residual microphone signals p_m, is performed:

$$\Phi^{(0)}(t,x_g) = b(t,x_g,\{p_m\}), \tag{3}$$

$$\Gamma^{(0)}(t,x_g) = 0, \tag{4}$$

$$p_m^{res(0)}(t) = p_m(t). \tag{5}$$

The strongest source in the defined search grid is then identified. The source that has the highest energy at x_g can be determined by integrating over a time frame T:

$$\hat{x}_g = \underset{x_g}{\operatorname{argmax}}(\int_T |\Phi^{(i-1)}(t,x_g)|^2 dt). \tag{6}$$

In the next step, this signal is added to the clean representation. Here, γ refers to the loop amplification factor that scales the size of the added signal.

$$\Gamma^{(i)}(t,\hat{x}_g) = \Gamma^{(i-1)}(t,\hat{x}_g) + \gamma\Phi^{(i-1)}(t,\hat{x}_g) \tag{7}$$

The microphone signals caused by this source signal are then modeled and subtracted from the remaining microphone signals.

$$p_m^{res(i)}(t+\frac{r_{x_g m}}{c}) = p_m^{res(i-1)}(t+\frac{r_{x_g m}}{c}) - \gamma\frac{\Phi^{(i-1)}(t,\hat{x}_g)}{r_{\hat{x}_g m}(t)(1-M\cos(\theta_{\hat{x}_g m}(t)))^2} \tag{8}$$

Here, M is the Mach number, and $\theta_{x_g,m}$ denotes the motion angle. The final step is beamforming with the updated residual microphone signals.

$$\Phi^{(i)}(t,x_g) = b(t,x_g,\{p_m^{res(i)}\}) \tag{9}$$

This process is repeated iteratively until the termination condition is reached, which can be defined as a certain number of iterations or when there is an increase in energy within the residual beamforming map.

3.3 Processing

The data were analysed using a specialised method based on the CLEANT technique [4], wherein the overall result is compiled from several partial results in a source map. Data processing was implemented using the Acoular [12] open-source Python package. The entire grid, on which the sources are reconstructed, has a length of 10 metres and a height of 4 metres. Individual grid points are defined at intervals of 0.1 metres, resulting in a grid comprising a total of 101 x 41 points and positioned on the surface area of the car facing the microphone array. Each sub-map has dimensions of 4 metres by 4 metres and consists of 41 x 41 grid points. The individual partial maps are multiplied by a horizontally aligned Hanning window and overlapped by 50 %. This process is illustrated in Figure 3. A total of four sub-maps, denoted as $\overline{M}_i$, are overlapped to generate the entire map.

To determine a sub-map, the measurement data are evaluated in signal blocks over a monitoring area. For further processing, a monitoring area from -1 m to 1 m in front of the array was chosen. Depending on the speed of the vehicle, this corresponds to an observation period. This process is visualised in the sketch shown in Figure 4. Here, the observation period consists of 5 signal blocks. Each block is evaluated separately, and the sub-map $\overline{M}$ is obtained as an average

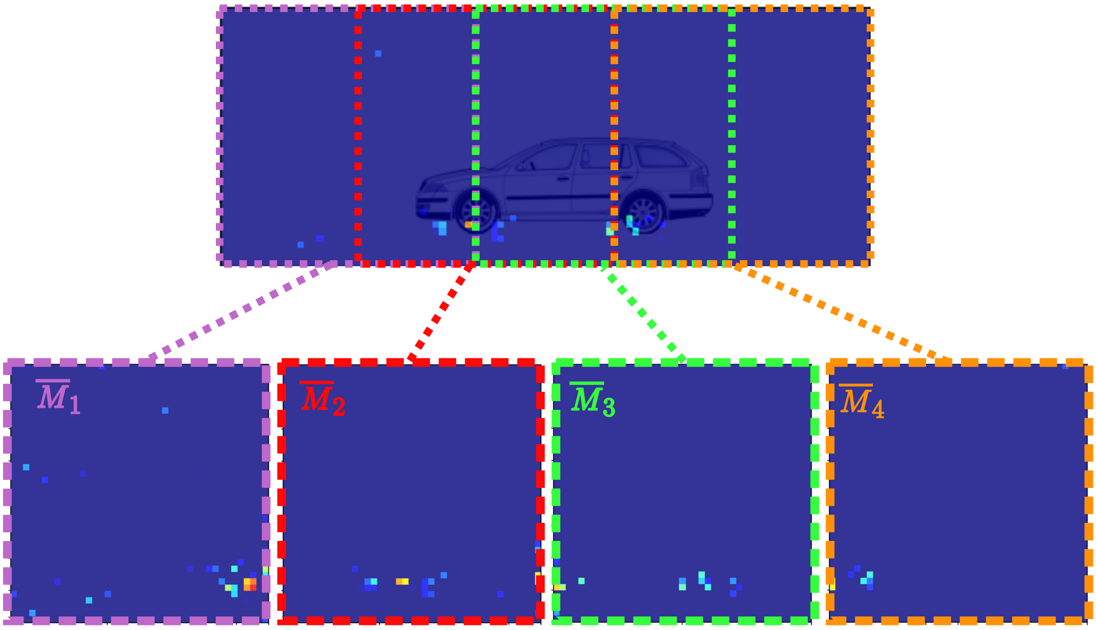

Figure 3: Sketch of the technique used to obtain a source map. Four sub-maps are overlapped to achieve the total source map.

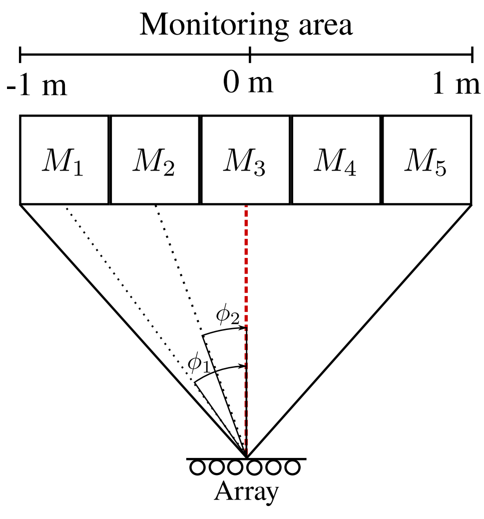

Figure 4: Evaluation of a sub-map from several observations (sub-sub-maps).

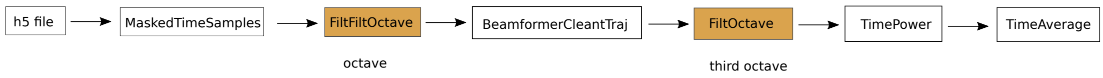

Figure 5: Acoular processing pipeline.

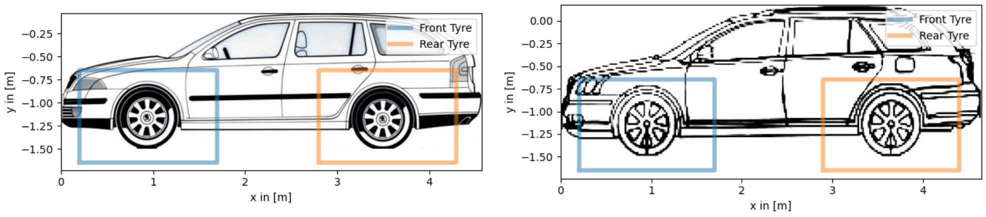

Figure 6: Defined integration sectors for the two cars: Skoda Octavia (left), Toyota Avensis (right).

of these results using the equation

$$\overline{M} = \frac{1}{5}\sum_{i=1}^{5} M_i. \tag{10}$$

After a sub-map $\overline{M}_i$ is obtained, the processing for the next sub-map $\overline{M}_{i+1}$ begins with a time sample delay equal to the time it would take the vehicle to travel half the distance of the sub-map. This ensures that the overlapping of the sub-maps results in a consistent source map.

The evaluation of a signal block uses the pipeline shown in Figure 5. Initially, the microphone data are filtered using an octave band filter, after which the CLEANT algorithm is applied with a loop gain factor of $\gamma = 0.8$. Finally, the data are filtered a second time using a one-third octave band filter. To determine the sound pressure level in the one-third octave band, the signal block is squared and averaged.

Two integration sectors are defined: ”Front Tyre” and ”Rear Tyre,” each measuring 1.5 metres in length and 1 metre in height. These sectors are centred on the wheels. Figure 6 illustrates these sectors for the two cars.

The spectra of these sectors are analyzed in greater detail, and the relationship between sound pressure level and vehicle speed is examined. A predictive function in the form of Equation (11) is derived from the results. The constants a_1 and a_2 are determined for each frequency band using linear regression. In this context, V represents the speed of the vehicle in km/h, and V_0 is a reference velocity set to 1 km/h.

$$L_p = a_1 + a_2 \log_{10}\left(\frac{V}{V_0}\right) \text{dB} \tag{11}$$

Additionally, the sound pressure level is expressed as a function of the Strouhal number (SR) according to equation

$$L_p = b_1 + b_2 \log_{10}(SR)\text{dB}. \tag{12}$$

Here, the constants b_1, b_2 are also determined by linear regression. The Strouhal number is defined by

$$SR = f\frac{L}{v}. \tag{13}$$

In this equation, f is the frequency in Hz, v is the speed of the vehicle in m/s, and L is the diameter of the tyre.

4 Results

Various example results are presented below, which can be determined using the method. These include a compilation of source maps, spectra, and a speed- and Strouhal number-dependent representation of the sound pressure levels. All levels presented are reconstructed at a distance of one metre from the grid points. It is important to note that these are not representative results, as the vehicles are old models and the measurements were not carried out in a controlled environment. Rather, the aim is to demonstrate the types of analyses possible using the method.

4.1 Source Maps

First, an exemplary selection of source maps is examined. Maps of the Skoda Octavia at nominal velocities of 30 km/h are shown in Figure 7, and at 80 km/h in Figure 8. In both cases, the one-third octave bands of 630 Hz, 1250 Hz, 2500 Hz, and 5000 Hz are displayed.

The source maps determined using the method demonstrate the source areas in a much more focused manner than when evaluated with beamforming with a moving focus. The dominant sources are concentrated at only a few points, whereas they would be distributed over many points when using beamforming.

In all source maps, noise sources occurring in the area of the wheels are identified as primary sources. At frequencies of 630 Hz and 1250 Hz, it can be observed that these sources are reconstructed slightly before and after the wheels. From 2500 Hz onwards, the sources are found to be more centred in the area of wheel-ground contact. When comparing source maps at the two speeds, it is noticeable that the sources are displayed with even greater focus at the higher speed. The sources between the wheels, occurring at 5000 Hz and 30 km/h, outside the dominant source areas, are not visible at the higher speed.

Studies referenced in [11] identify noise sources in tyre/road interactions using techniques such as sound intensity and vibration measurements, near-field acoustic holography, and spatial sound field transformation. The findings indicate that noise sources are primarily located near

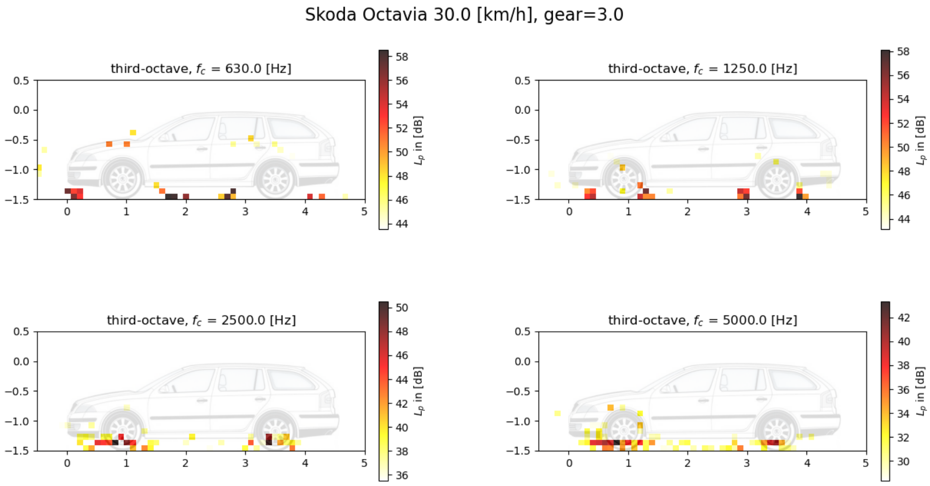

Figure 7: Example source maps for different one-third octave bands for a pass-by of the Skoda Octavia at a speed of 30 km/h.

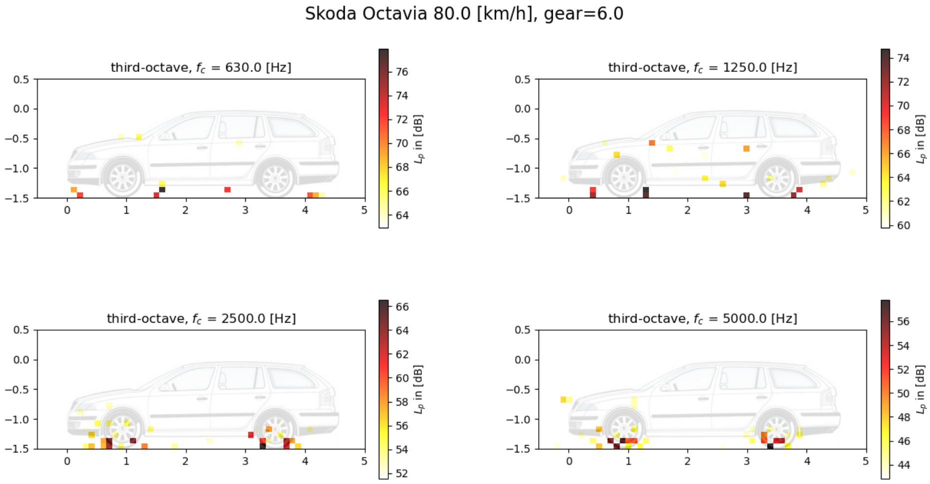

Figure 8: Example source maps for different one-third octave bands for a pass-by of the Skoda Octavia at a speed of 80 km/h.

the leading and trailing edges of the tyre, particularly at the tread centre, with slightly higher emissions from the front of the tyre compared to the rear. The source distributions observed in the source maps are consistent with these observations and were similarly found in the evaluations by Ballesteros et al. [1, 2].

4.2 Spectra

Figure 9 presents an exemplary depiction of the sound pressure level for the ”Front Tyre” and ”Rear Tyre” sectors in the one-third octave band for nominal speeds ranging from 30 km/h to 80 km/h for both vehicles. The displayed level represents the average value of all pass-bys at the specified nominal speed using the same gear. It is observed that all curves exhibit a similar downward slope with frequency, peaking at 1000 Hz. A general increase in the one-third octave band level of up to 15 dB is observed with the increase in speed from 30 km/h to 80 km/h. The spectra of the Skoda Octavia and Toyota Avensis are very similar, with the most significant differences occurring at the nominal speed of 30 km/h, where the ”Front Tyre” sector of the Toyota Avensis shows approximately 3 dB higher levels for frequencies upwards of 1600 Hz. At higher speeds, these differences diminish, with certain areas showing the Skoda Octavia having a larger sound pressure level, such as at 50 km/h from 2500 Hz by about 2 dB. These differences may be attributed to the utilisation of a diesel engine in the Toyota Avensis, which predominantly contributes to noise levels at lower speeds.

A similar trend can be observed when comparing the level of the ”Front Tyre” sector with the level of the ”Rear Tyre” sector. At a speed of 30 km/h, higher levels are reconstructed for the ”Front Tyre” sector, particularly at frequencies above 1600 Hz. For the Toyota Avensis, these levels are approximately 6 dB higher, and for the Skoda Octavia, they are up to 4 dB higher. At higher speeds, these differences become smaller, being in the order of approximately 2 dB at speeds of 60 km/h and above.

The spectra exhibit a pattern similar to those reported in the literature [11], with a peak between 800 Hz and 1000 Hz. This peak is attributed to tyre tread patterns, groove resonances, Helmholtz resonance, and the horn effect.

4.3 Speed Dependence

To investigate the speed dependency, the sound pressure level for both sectors is presented as a function of speed in Figure 10 for the ”Front Tyre” sector and in Figure 11 for the ”Rear Tyre” sector. In each subfigure, the results from pass-by measurements at all nominal velocities using the highest gear are shown as individual data points. The results of the prediction function, as defined by Equation (11), are calculated separately for each vehicle and in each one-third octave band using linear regression. This prediction function is then depicted as a continuous line. Additionally, the root mean square error (RMSE) is calculated between the prediction function and the individually obtained level values.

The results indicate that fluctuations in levels are most pronounced in the one-third octave band at 630 Hz. In this band, the RMSE reaches its highest value of 2.4 dB in the ”Rear Tyre” sector of the Skoda Octavia. In other one-third octave bands, these deviations are smaller, with the RMSE being approximately 1 dB for the ”Front Tyre” sector and 0.7 dB for the ”Rear Tyre” sector.

The obtained values for the constant a_2 of the prediction function range between 20 and 40. These values align with those reported in the literature [17].

The observations in the one-third octave band at 630 Hz could be attributed to the dominant source areas being located near the sector boundaries, as illustrated in source maps. Deviations during pass-by events may cause these areas to be reconstructed either within the sector or outside of it, leading to the observed discrepancies.

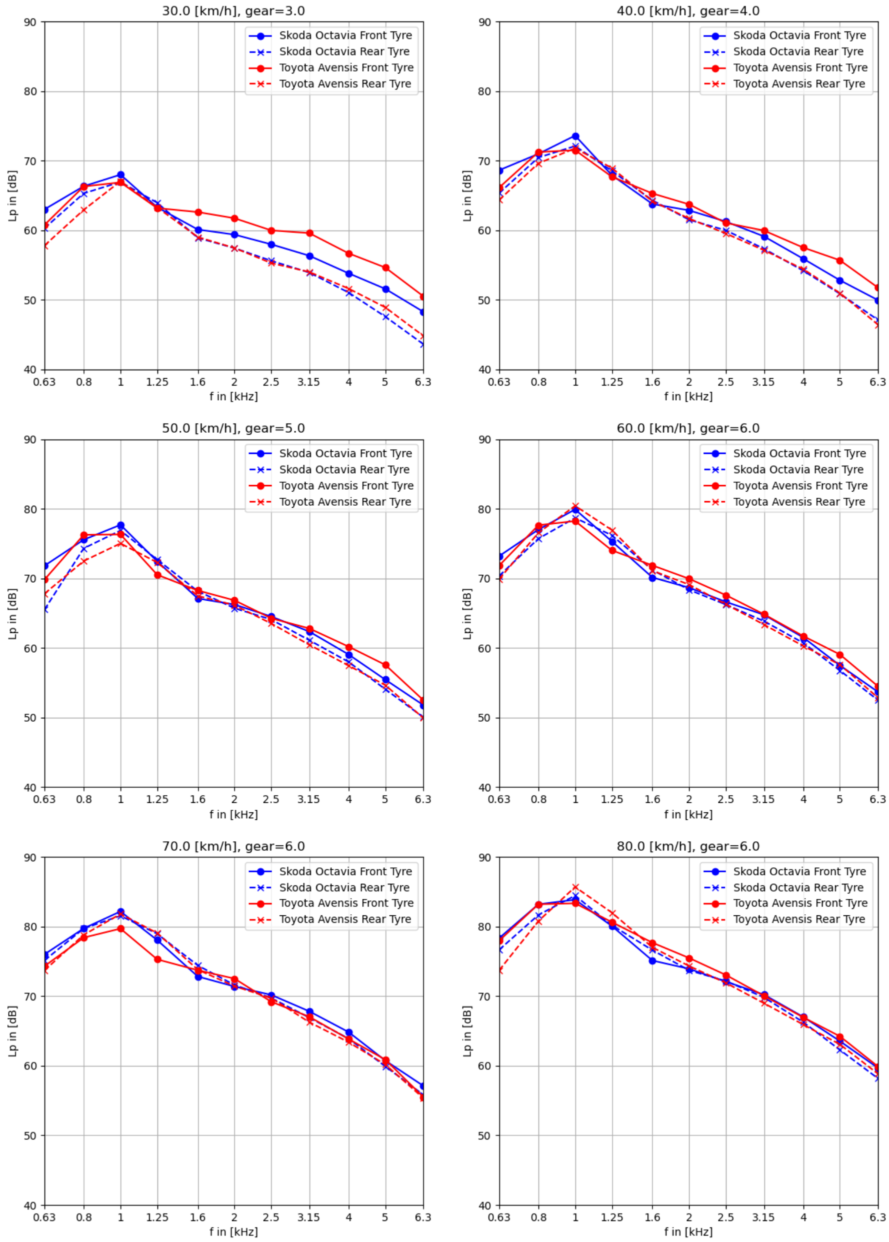

Figure 9: Example sound pressure levels in the "Front Tyre" and "Rear Tyre" integration sectors at different velocities for the Skoda Octavia and the Toyota Avensis. The level is averaged over all pass-bys with the same nominal speed.

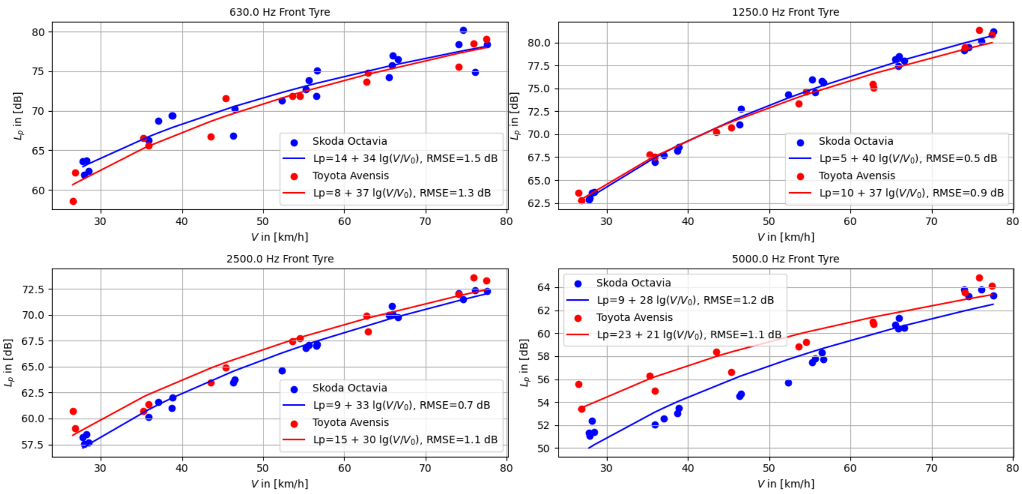

Figure 10: Example sound pressure levels of the "Front Tyre" sector depending on the driving speed for different one-third octave bands and cars. The obtained prediction function is depicted as a solid line.

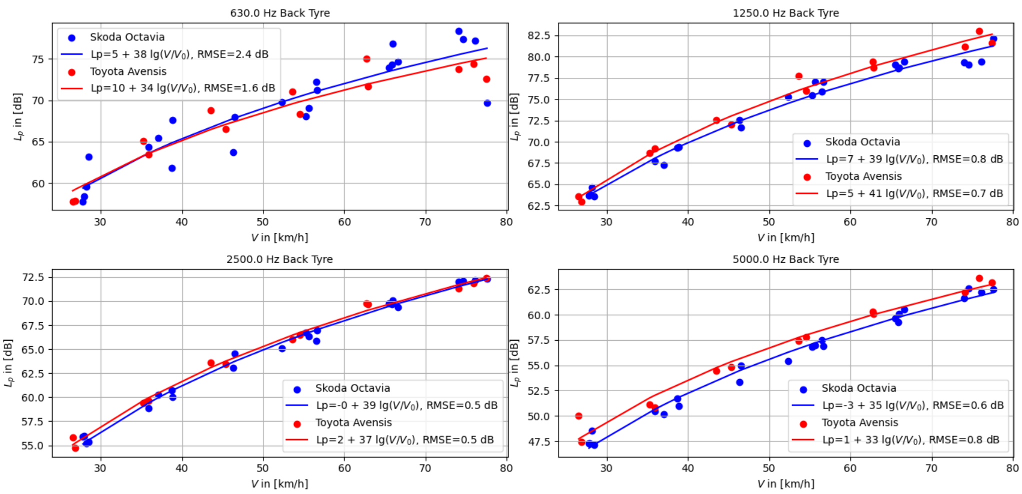

Figure 11: Example sound pressure levels of the "Rear Tyre" sector depending on the driving speed for different one-third octave bands and cars. The obtained prediction function is depicted as a solid line.

4.4 Strouhal Number Dependence

In a similar investigation, the sound pressure levels across the two sectors of both vehicles are depicted as a function of the Strouhal number. Data encompassing all nominal velocities, while employing the highest transmission gear, and within the frequency spectrum ranging

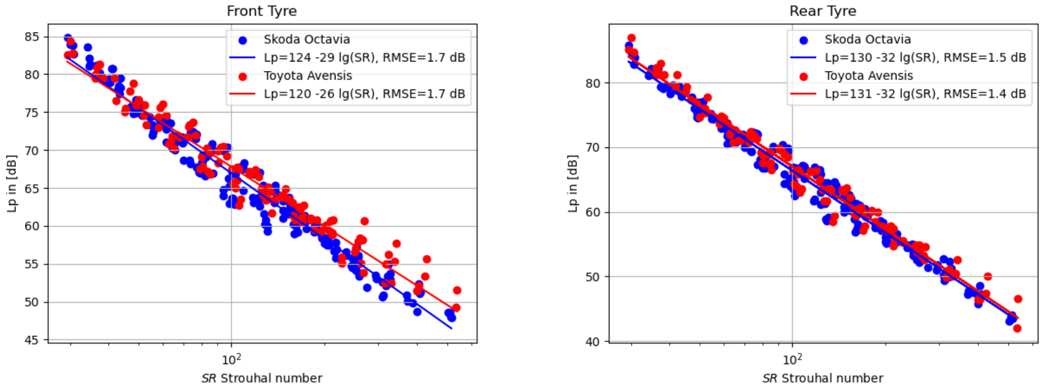

Figure 12: Example sound pressure levels of the "Front Tyre" sector (left) and "Rear Tyre" sector (right) depended on Strouhal number depicted for the two different cars. The prediction function is depicted as a solid line.

from 1000 Hz to 6300 Hz, were utilized. In Figure 4.4, the obtained levels are represented by points, and the predictive function, derived in accordance with Equation (12), is depicted as a continuous line. Additionally, RMSE between the observed values and the predictive function was calculated.

Subsequent calculations yield RMSE values of 1.4 dB and 1.7 dB, with the sector labeled "Front Tyre" exhibiting the higher values. Regarding the constant b_2 of the predictive function, obtained values range between -26 and -32.

5 Conclusion

The application of the CLEANT deconvolution method, employing multiple sub-maps, was successfully demonstrated on vehicle pass-by data. The reconstructed source maps identified predominant sources at the tyre/road contact area. At higher frequencies, these sources were concentrated around the tyre, whereas at lower frequencies, they were predominantly located near the leading and trailing edges of the tyre. Compared to beamforming with a moving focus, this method achieved significantly enhanced source localisation by reconstructing the sources on a limited number of grid points.

The method provides a tool that enables different spatially or frequency-separated source areas to be examined independently. This allows the independent investigation of various dependencies within these areas. For example, this could involve examining the influence of velocity or Strouhal number, as demonstrated here, but other influencing variables such as temperature or material properties could also be investigated in this manner.

However, to obtain representative results, the measurements should be conducted on a test track where potential interferences can be controlled. For instance, it is essential to precisely control the vehicle condition, speed, tyres, road condition, and any possible sources of interference during the measurement. Additionally, a comparison, such as that conducted in the TRANSIT project [15], should be made with a single microphone measurement to independently verify the results.

The exemplary findings were consistent with those reported in the literature and previous studies, suggesting that the method is appropriate for analyzing automobile pass-by noise.

References

[1] J. Ballesteros, E. Sarradj, M. Fernandes, T. Geyer, and M. Ballesteros. "Methodology for pass-by measuremtns with beamforming on cars." In *Proceedings on CD of the 5th Berlin Beamforming Conference, 19-20 February 2014*. GFaI, Gesellschaft zu Förderung angewandter Informatik e.V., Berlin, 2014. ISBN 978-3-942709-12-5. URL `http://bebec.eu/Downloads/BeBeC2014/Papers/BeBeC-2014-30.pdf`.

[2] J. A. Ballesteros, E. Sarradj, M. D. Fernández, T. Geyer, and M. J. Ballesteros. "Noise source identification with beamforming in the pass-by of a car." *Applied Acoustics*, 93, 106–119, 2015. ISSN 0003-682X. doi:https://doi.org/10.1016/j.apacoust.2015.01.019. URL `https://www.sciencedirect.com/science/article/pii/S0003682X15000304`.

[3] M. Braun, S. Walsh, J. Horner, and R. Chuter. "Noise source characteristics in the iso 362 vehicle pass-by noise test: Literature review." *Applied Acoustics*, 74(11), 1241–1265, 2013. ISSN 0003-682X. doi:https://doi.org/10.1016/j.apacoust.2013.04.005. URL `https://www.sciencedirect.com/science/article/pii/S0003682X13000790`.

[4] R. Cousson, Q. Leclère, M.-A. Pallas, and M. Bérengier. "A time domain clean approach for the identification of acoustic moving sources." *Journal of Sound and Vibration*, 443, 47–62, 2019. ISSN 0022-460X. doi:https://doi.org/10.1016/j.jsv.2018.11.026. URL `https://www.sciencedirect.com/science/article/pii/S0022460X18307880`.

[5] M. Czuchaj, S. Jekosch, A. Kujawski, and E. Sarradj. "Quantitative Charakterisierung von Schallquellen mit Mikrofonarrays bei der Vorbeifahrt von Zügen." In *Fortschritte der Akustik - DAGA 2023, 49. Jahrestagung für Akustik*, pages 365–368. Deutsche Gesellschaft für Akustik e.V. (DEGA), Hamburg, 2023. ISBN 978-3-939296-21-8.

[6] M. Czuchaj, A. Kujawski, and E. Sarradj. "Erweiterung der CLEANT-Methode zur Entfaltung bei Mikrofonarray-Messungen an Hochgeschwindigkeitszügen." In *Fortschritte der Akustik - DAGA 2021, 47. Jahrestagung für Akustik*. Deutsche Gesellschaft für Akustik e.V. (DEGA), Wien, 2021. ISBN 978-3-939296-18-8.

[7] A. Kujawski and E. Sarradj. "Application of the CLEANT Method for High Speed Railway Train Measurements." In *Proceedings on CD of the 8th Berlin Beamforming Conference*, pages 1–13. Gesellschaft zur Förderung angewandter Informatik (GFaI), Berlin, 2020. ISBN 978-3-942709-22-4. URL `https://www.bebec.eu/fileadmin/bebec/downloads/bebec-2020/papers/BeBeC-2020-D02.pdf`.

[8] M. Li, S. Zhong, T. Deng, Z. Zhu, and X. Sheng. "Analysis of source contribution to pass-by noise for a moving high-speed train based on microphone array measurement." *Measurement*, 174, 109058, 2021. ISSN 0263-2241. doi:https://doi.org/10.1016/j.measurement.2021.109058. URL `https://www.sciencedirect.com/science/article/pii/S0263224121000907`.

[9] R. Merino-Martinez, M. Snellen, and D. Simons. "Functional beamforming applied to full scale landing aircraft." In *Proceedings on CD of the 6th Berlin Beamforming Conference, 29th February - 1st March 2016*. GFaI, Gesellschaft zu Förderung angewandter Informatik e.V., Berlin, 2016. ISBN 978-3-94270915-6. URL `http://www.bebec.eu/Downloads/BeBeC2016/Papers/BeBeC-2016-D12.pdf`.

[10] H.-M. Noh, S. Choi, S. Hong, and S.-w. Kim. "Investigation of noise sources in high-speed trains." *Proceedings of the Institution of Mechanical Engineers, Part F: Journal of Rail and Rapid Transit*, 228, 307–322, 2014. doi:10.1177/0954409712473095.

[11] U. Sandberg and J. Ejsmont. *Tyre/road Noise Reference Book*. INFORMEX, 2002. ISBN 9789163126109. URL `https://books.google.de/books?id=yQW9AAAACAAJ`.

[12] E. Sarradj and G. Herold. "A python framework for microphone array data processing." *Applied Acoustics*, 116, 50–58, 2017. ISSN 0003-682X. doi:https://doi.org/10.1016/j.apacoust.2016.09.015. URL `https://www.sciencedirect.com/science/article/pii/S0003682X16302808`.

[13] T. Schumacher and H. Siller. "Hybrid approach for deconvoluting tonal noise of moving sources." In *Proceedings on CD of the 9th Berlin Beamforming Conference, 8-9 June, 2022*. 2022. URL `https://www.bebec.eu/fileadmin/bebec/downloads/bebec-2022/papers/BeBeC-2022-D01.pdf`.

[14] TRANSIT Consortium. "Innovative separation techniques: theoretical description and validation testing campaign proposal, deliverable d2.2.", 2022. URL `https://projects.shift2rail.org/s2r_ipCC_n.aspx?p=S2R_TRANSIT`.

[15] TRANSIT Consortium. "Analysis of pass-by source separation results and uncertainty analysis; innovative separation techniques: validation test results, deliverable d2.4.", 2023. URL `https://projects.shift2rail.org/s2r_ipCC_n.aspx?p=S2R_TRANSIT`.

[16] TRANSIT Consortium. "Measurement plan and database of raw and processed data, deliverable d2.3.", 2023. URL `https://projects.shift2rail.org/s2r_ipCC_n.aspx?p=S2R_TRANSIT`.

[17] J. Winroth, W. Kropp, C. Hoever, T. Beckenbauer, and M. Männel. "Investigating generation mechanisms of tyre/road noise by speed exponent analysis." *Applied Acoustics*, 115, 101–108, 2017. ISSN 0003-682X. doi:https://doi.org/10.1016/j.apacoust.2016.08.027. URL `https://www.sciencedirect.com/science/article/pii/S0003682X16302523`.